Atmos. Chem. Phys., 20, 6115–6128, 2020
https://doi.org/10.5194/acp-20-6115-2020

Atmospheric Chemistry and Physics
Open Access
EGU

Molecular composition and photochemical evolution of water-soluble organic carbon (WSOC) extracted from field biomass burning aerosols using high-resolution mass spectrometry

Jing Cai[1,2], Xiangying Zeng[1], Guorui Zhi[3], Sasho Gligorovski[1], Guoying Sheng[1], Zhiqiang Yu[1], Xinming Wang[1], and Ping'an Peng[1]

[1]State Key Laboratory of Organic Geochemistry, Guangdong Key Laboratory of Environment and Resources, Guangzhou Institute of Geochemistry, Chinese Academy of Sciences, Guangzhou, 510640, China
[2]University of Chinese Academy of Sciences, Beijing, 100049, China
[3]State Key Laboratory of Environmental Criteria and Risk Assessment, Chinese Research Academy of Environmental Sciences, Beijing, 100012, China

Correspondence: Zhiqiang Yu (zhiqiang@gig.ac.cn)

Received: 27 June 2019 – Discussion started: 14 October 2019
Revised: 14 April 2020 – Accepted: 17 April 2020 – Published: 26 May 2020

Abstract. Photochemistry plays an important role in the evolution of atmospheric water-soluble organic carbon (WSOC), which dissolves into clouds, fogs, and aerosol liquid water. In this study, we tentatively examined the molecular composition and evolution of a WSOC mixture extracted from field-collected wheat straw burning aerosol (WSBA) samples upon photolysis, using direct infusion electrospray ionisation (ESI) coupled to high-resolution mass spectrometry (HRMS) and liquid chromatography (LC) coupled with HRMS. For comparison, two typical phenolic compounds (i.e. phenol and guaiacol) emitted from lignin pyrolysis in combination with hydrogen peroxide (H_2O_2) as a typical OH radical precursor were simultaneously exposed to simulated sunlight irradiation. Their photochemical products such as phenolic dimers (e.g. m/z 185.0608 for phenol dimer and m/z 245.0823 for guaiacol dimer) or their isomers, were also observed in field-collected WSBA samples, suggesting that the aqueous-phase reactions might contribute to the formation of emitted biomass burning aerosols. The aqueous photochemistry of both the phenols (photooxidation) and WSBA extracts (direct photolysis) could produce a series of highly oxygenated compounds, which in turn increases the oxidation degree of organic composition and acidity of the bulk solution. In particular, the LC/ESI-HRMS technique revealed significant photochemical evolution of the WSOC composition in WSBA samples, e.g. the photodegradation of low oxygenated species and the formation of highly oxygenated products. We also tentatively compared the mass spectra of photolytic time-profile WSBA extracts with each other for a more comprehensive description of the photolytic evolution. The calculated average oxygen-to-carbon ratio (O/C) of oxygenated compounds in bulk extract increases from 0.38 ± 0.02 to 0.44 ± 0.02 (mean $\pm$ standard deviation), while the intensity (S/N)-weighted average O/C (O/C_w) increases from 0.45 ± 0.03 to 0.53 ± 0.06 as the time of irradiation extends from 0 to 12 h. These findings indicate that the water-soluble organic fraction of combustion-derived aerosols has the potential to form more oxidised organic matter, contributing to the highly oxygenated nature of atmospheric organic aerosols.

1 Introduction

Water-soluble organic carbon (WSOC) comprises a significant fraction of atmospheric aerosols, accounting for 20 %–80 % of total organic carbon (OC) (Krivacsy et al., 2001; Wozniak et al., 2008; Fu et al., 2015; Xie et al., 2016). WSOC is directly involved in the formation of cloud condensation nuclei (CCN) by modifying the aqueous chemistry and surface tension of cloud droplets (Graham et al., 2002; Nguyen et al., 2012; Zhao et al., 2013; McNeill, 2015). De-

spite its significance, little is known about the chemical composition and sources of WSOC, with less than 10 %–20 % of the organic mass being structurally identified (Cappiello et al., 2003; Fu et al., 2015). Biomass burning is a well-known emission source of WSOC (Anastasio et al., 1997; Fine et al., 2001; Graham et al., 2002; Mayol-Bracero et al., 2002; Gilardoni et al., 2016). Although the composition varies with fuel type and combustion conditions (Simoneit, 2002; Smith et al., 2009), the WSOC mixture often covers a common range of polar and oxygenated aromatic compounds (Graham et al., 2002; Mayol-Bracero et al., 2002; Duarte et al., 2007; Chang and Thompson, 2010; Yee et al., 2013; Gilardoni et al., 2016) with molecules incorporating different numbers of functional groups like hydroxyl, carboxyl, aldehyde, ketone, ester, amino, and/or other nitrogen-containing groups (Graham et al., 2002). In particular, lignin pyrolysis often yields a large amount of aromatic alcohols, carbonyls, and acid compounds (Mayol-Bracero et al., 2002; Chang and Thompson, 2010; Gilardoni et al., 2016). Once dissolved into cloud, fog, and even aerosol liquid water, these substances can undergo aqueous-phase reactions to generate low-volatility species under sunlight irradiation, which have the potential to form secondary organic aerosol (SOA) after water evaporation (Graham et al., 2002; Cappiello et al., 2003; Duarte et al., 2007; Sun et al., 2010; Yu et al., 2014).

Field and laboratory studies have demonstrated that aqueous photochemical processes contribute significantly to the aqueous SOA formation from biomass burning precursors and the evolution of smoke particles (Sun et al., 2010; Lee et al., 2011; Kitanovski et al., 2014; Yu et al., 2014; McNeill, 2015; Gilardoni et al., 2016). Gilardoni et al. (2016) observed aqueous SOA formation in both fog water and wet aerosols, resulting in an enhancement in the oxidised organic aerosol, and following atmospheric ageing the overall oxidation degree of aerosols has also increased. In laboratory studies, phenols and methoxyphenols (important biomass burning intermediates) are often used as SOA precursors to examine the photochemical evolution in aqueous environments and aerosol-forming potential under relevant atmospheric conditions (Chang and Thompson, 2010; Sun et al., 2010; Smith et al., 2014; Yu et al., 2014; Vione et al., 2019). The corresponding photochemical products formed through hydroxylation, oligomerisation, and fragmentation typically cover a series of low-volatility and highly oxygenated species. For instance, the methoxyphenol-derived SOA are proposed as a proxy for atmospheric humic-like substances (HULIS) (Ofner et al., 2011; Yee et al., 2013). Other compounds emitted from lignin pyrolysis, e.g. aromatic aldehydes, ketones, polycyclic aromatic hydrocarbon (PAH), have also been found to produce coloured products via aqueous photooxidation, which may become a part of HULIS (Anastasio et al., 1997; Chang and Thompson, 2010; Haynes et al., 2019). In addition, photochemical processing of common water-soluble aliphatic compounds such as aldehydes (Lim and Turpin, 2015), polyols (Daumit et al., 2014), and organic acids (Griffith et al., 2013) in aqueous solution can also lead to the formation of oligomers, highly oxygenated, and multifunctional organic matter (McNeill, 2015).

In recent years, high-resolution mass spectrometry (HRMS) has been commonly applied to study the organic molecular composition in cloud water (Zhao et al., 2013; Boone et al., 2015), fog water (Cappiello et al., 2003), rainwater (Altieri et al., 2009a, b), laboratory-generated SOA (Bateman et al., 2011; Romonosky et al., 2015; Lavi et al., 2017), and field-collected aerosol samples (Laskin et al., 2009; Lin et al., 2012a, b; Kourtchev et al., 2013; Tong et al., 2016; Wang et al., 2017). It has also been used in time-profile observations of the photochemical evolution of aqueous extracts from laboratory-generated SOAs (Bateman et al., 2011; Romonosky et al., 2015). However, direct infusion mass spectrometry (MS) methods are prone to ion suppression caused by other organic species, inorganic salts, and adduct formation (Kourtchev et al., 2013). Therefore, liquid chromatography (LC) coupled with HRMS might be another complementary powerful tool for relieving ion suppression due to its abilities to separate and analyse different kind of compounds with differences in LC retention time (Kourtchev et al., 2013; Wang et al., 2016). It could also provide more information enabling the identification of possible isomers from the ions with same mass-to-charge ratio (m/z).

To our knowledge, the aqueous photochemical evolution of WSOC extracted from real ambient aerosols has not been studied in detail at the molecular level. Our previous study has revealed that the ultraviolet–visible (UV–vis) absorption spectra of aqueous extracts from field biomass burning aerosols were modified under simulated sunlight illumination (Cai et al., 2018). Based on the previously studied field-collected samples, the present study is focused on a further analysis to investigate the molecular characteristics of water-soluble organic molecules by the photochemical evolution using electrospray ionisation (ESI)-HRMS and LC/ESI-HRMS performed in negative ionisation mode. For comparison, we also evaluated the photochemistry of phenol and guaiacol (representing the basic structures of phenols emitted from lignin pyrolysis) under laboratory conditions, and tentatively traced some of their photochemical products (e.g. dimers) in field-collected samples under study.

2 Experimental section

2.1 Particulate sample collection and preparation of aqueous extracts

The wheat straw burning aerosol (WSBA) samples were collected during the summer harvest season of 2013, at rural fields in the plain of north China where the wheat was the main agricultural crop (Cai et al., 2018). To facilitate subsequent planting and management, a large amount of fresh wheat straw was directly burned in the field during

Figure 1. One field site at Daming, Hebei province, China, for sampling the aerosols affected by biomass burning.

the harvest season, and the water emitted from burning plant body could provide a suitable environment for aqueous photochemistry of dissolved compounds. The selected WSBA samples used for HRMS analysis were collected from two sampling sites, located at rural fields in Wenxian in Henan Province (denoted: HNWX) and Daming in Hebei Province (HBDM). As described in Cai et al. (2018), the selected sampling sites were mainly affected by heavy smog from wheat straw burning (Fig. 1). The emitted fine particulate matter with aerodynamic diameter $\leq 2.5\,\mu m$ ($PM_{2.5}$) was collected at a flow rate of $5\,L\,min^{-1}$ by a portable particulate sampler (MiniVol TAS, AirMetrics, USA), with quartz fibre filters (47 mm in diameter, QMA, Whatman, UK) baked at 600 °C for 6 h before sampling. The sampling flow rate was calibrated with a standard flow meter (Bios Defender 520), and the sampling time of each filter was restricted to 30–60 min depending on the ambient biomass burning aerosol concentration and expected filter loading (Cai et al., 2018). After collection, the filter samples were stored in the dark and transported to the laboratory and then stored at −20 °C under light-proof conditions.

The preparation of WSOC extracts and measurements for carbon content including OC, elemental carbon (EC) (Zhi et al., 2014) and WSOC were described in detail in Cai et al. (2018). Briefly, a part of each quartz fibre filters (1.6–3.2 cm^2) was placed in a brown vial and extracted with ultrapure water (Milli-Q, Milipore) twice; each time 5 mL ultrapure water with a 30 min ultrasonic agitation was applied. The two-time extracts were combined and filtered through a PTFE syringe filter (0.2 µm pore size, Thermo Scientific), followed by a pH measurement with a pH meter (Mettler Toledo SevenEasyTM S20) that had been regularly calibrated at pH 4.00 and 6.86. Prior to analysis the extracts were stored at −20 °C in the dark. To reduce the WSOC mass loss, the desalting treatment (e.g. solid phase extraction, SPE) was not performed on these samples.

2.2 Direct photolysis of WSOC extracts

A 12 h direct photolysis of WSOC extracts obtained from WSBA samples was performed in a photo-reactor (BL-GHX-V, Bilon Instruments Co. Ltd., China; see Fig. S1 in the Supplement) that was equipped with a solar simulator (Xe lamp, 1000 W) placed in a double-deck quartz condenser (Cai et al., 2018). Cooling water (18 °C) was circulating in the outer tube of the condenser to avoid heating of the samples. In the wavelength range of 310–400 nm relevant to the boundary layer of the atmosphere, the actinic flux of the lamp is about 5 times stronger than the solar actinic flux, meaning that the spectral evolution via the 12 h simulated solar irradiation might be equal with the effect caused by actual sunlight irradiation with a duration of at least 60 h (Cai et al., 2018). Airtight quartz tubes (1.5 cm in diameter, 3 mL solution per tube) loading extracts were equidistantly arranged around the lamp. Each extract was distributed into three tubes that corresponded to three different irradiation times, i.e. 0, 4, and 12 h, with no oxidants added externally throughout the whole photolytic process. At each irradiation time point (e.g. 0 and 4 h), the related tubes were wrapped with aluminium foil and placed in the initial location until the end of the 12 h photolysis (Cai et al., 2018).

As described in Cai et al. (2018), the water extraction resulted in a dilution of the collected organic compounds; however, the ratio of the water mass to $PM_{2.5}$ mass for extract samples (ranging from 1.8×10^3 to 3.4×10^4) was compatible with the ratio of water mass to WSOC content in cloud water (in a wide range from 1.4×10^2 to 1.6×10^4) (Li et al., 2017), indicating that the present aqueous extracts are relevant to the atmospheric cloud water condition.

2.3 Photooxidation of phenolic compounds under laboratory conditions

Initial solutions of 0.1 mM phenol (C_6H_6O) and 0.1 mM guaiacol ($C_7H_8O_2$) in combination with an OH radical precursor (0.1 mM H_2O_2) were prepared in ultra-pure water (Milli-Q, Milipore). The pH of the solution was adjusted to 5 with 0.1 M sulfuric acid (H_2SO_4), which is usually relevant to the acidity in fog and cloud waters (Collet et al., 1998; Fahey et al., 2005). The prepared solution and reference blank were irradiated by simulated sunlight irradiation with a duration of 4 h. Hereby, we mainly focus on acquiring the chemical characteristics of aqueous products of phenols and tentatively identify whether certain tracer compounds (e.g. phenolic dimers) exist in the present biomass burning particulate samples.

2.4 Sample analysis

The direct infusion MS analysis was conducted using a Thermo Scientific Orbitrap Fusion Tribrid mass spectrometer equipped with quadrupole, orbitrap, and linear ion trap

mass analysers, with a heated ESI source. To assist in ionisation and desolvation, the sample was diluted to a 1 : 1 mixture of acetonitrile and sample by volume. The full scan mass spectra were acquired in negative ionisation mode, with a resolution of 120 000 at m/z 200 for the Orbitrap analyser and a mass scan range of m/z 50–750. Before determination, the Orbitrap analyser was externally calibrated for mass accuracy using a Thermo Scientific Pierce LTQ Velos ESI calibration solution. The direct infusion parameters were as follows: sample flow rate 5 µL min^{-1}; capillary temperature 300 °C; S-lens RF 65 %; spray voltage −3.5 kV; sheath gas, auxiliary gas, and sweep gas flows were 10, 3, and 0 arbitrary units, respectively. Data collecting was performed when the intensity of the total ion current (TIC) maintained constant with a relative standard deviation (RSD) under 5 %. At least 100 data points (mass spectral scans) were collected for each test sample, and each exported mass spectrum for analysis was derived from the average result of 100 spectra.

The LC/ESI-HRMS analysis operated in negative ionisation mode was performed using a U3000 system coupled with a T3 Atlantis C18 column (3 µm; 2.1 × 150 mm; Waters, Milford, USA) and an Orbitrap Fusion MS. A 10 µL sample was injected, with a flow rate of 0.2 mL min^{-1} for the mobile phase, which consisted of H_2O (A) and acetonitrile (B). The gradient applied was 0–5 min at 3 % B and 5–20 min from 3 % to 95 % (linear); it was then kept for 25 min at 95 %; then 45–50 min from 95 % to 3 %, and it was then held for 10 min at 3 % (total run time 60 min).

2.5 Data processing

Mass spectral peaks 3 times larger than the signal-to-noise ratio (S/N) were extracted from the raw files. Peaks in both sample and blank spectra were retained if their intensity in the former was 5 times larger than in the latter. A common molecular assignment based on the accurate mass was performed using Xcalibur software (V3.0 Thermo Scientific) with the following constraints: $^{12}C \leq 50$, $^{13}C \leq 1$, $^{1}H \leq 100$, $^{16}O \leq 50$, $^{14}N \leq 4$, $^{32}S \leq 1$, and $^{34}S \leq 1$. All mathematically possible elemental formulas, with a mass tolerance of ±3 ppm were calculated. Elemental formulas containing ^{13}C or ^{34}S were checked for the presence of ^{12}C or ^{32}S counterparts, respectively. If they were not matched with the corresponding mono-isotopic formulas, then the assignment to the next larger mass error was considered. Isotopic and unassigned peaks were excluded from further analysis.

Ions were also characterised by the number of rings plus double bonds (i.e. double-bond equivalents, DBEs), which were calculated as $\mathrm{DBE} = c - h/2 + n/2 + 1$ for an elemental composition of $C_cH_hO_oN_nS_s$. The assigned formula was additionally checked with the nitrogen rule. For ambient samples, based on the presence of various elements in a molecule, the identified elemental formulas were classified into several main compound classes: CHO (i.e. molecules containing only C, H, and O atoms), CHOS, CHON, and CHONS, and others including CHN and CHS. In the present study, because the detected water-soluble ions almost were below m/z 400, we focused our molecular analysis on m/z 50–400.

3 Results and discussion

3.1 Mass spectral characteristics of WSOC extracts from WSBA samples

The preliminary analysis showed that the $PM_{2.5}$ concentration in ambient air near the burning sites ranged from 6.46 to 28.03 mg m^{-3} (Table S1 in the Supplement). OC was the major component of the collected $PM_{2.5}$ with a proportion of 50.9 ± 7.6 % (mean ± standard deviation), whereas EC represented a negligible fraction (average 1.3 ± 0.4 %). Meanwhile, WSOC accounted for 35.5 ± 7.5 % of OC in the tested samples.

Although this batch of aerosol samples were collected from different sites, their water-extracted solutions showed similar light-absorbing characteristics in UV–vis absorption spectra (Cai et al., 2018). Here, four extract samples (HNWX-1, HNWX-2, HBDM-1, and HBDM-2) (Table S1) were chosen for further analysis using high-resolution mass spectrometry. These samples also exhibited similar patterns in mass distribution of water-soluble molecular species that mainly range from 50 to 400 Da, which indicated a similar burning source for these samples. A reconstructed mass spectrum (subtracted blank) for one representative sample of HNWX-1 is shown in Fig. 2a (others are shown in Fig. S2). In the mass range of 50–400 Da, there were 827 ± 44 molecular formulas identified throughout the all samples, and most of the formulas (above 75 %) overlapped between these analysed samples. The classification features of assigned compounds for analysed extracts are shown in Table S2. In the amount of assigned formulas, CHO composition was the most abundant group, accounting for 59.2 ± 2.2 % of the total assignments, followed by CHON (35.0 ± 2.2 %). These results are consistent with previous observations of laboratory-generated biomass burning aerosol (Smith et al., 2009) and field particulate samples influenced by biomass combustion (Kourtchev et al., 2016) in spite of the differences of biomass varieties, extracted solvents, and HRMS techniques between present and previous studies.

On the other hand, CHOS and CHONS compounds contributed with less than 5 % to the total assignment. A number of studies have shown the wide presence of organosulfates and nitrooxy-organosulfates in urban (Lin et al., 2012b; Wang et al., 2016), rural (Lin et al., 2012a), and forest aerosols (Kourtchev et al., 2013) and even in cloud water (Boone et al., 2015); however, most of these compounds were not observed in our negative mass spectra. This could be accounted for by the low extent of aerosol evolution, due to the limited oxidation conditions available for the formation

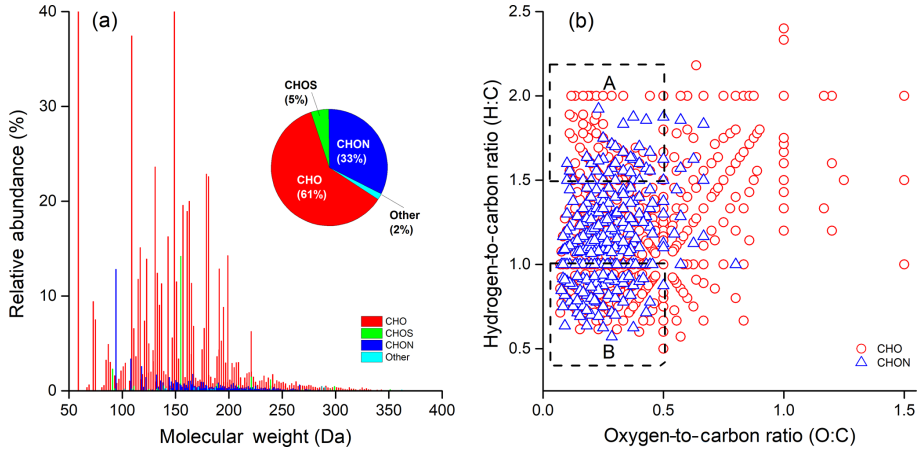

Figure 2. **(a)** Reconstructed mass spectra for detected ions with assigned formulas and **(b)** Van Krevelen diagrams for CHO and CHON species in extract of HNWX-1 sample. The inset pie charts in **(a)** show the number fraction of each class in the total assigned compounds. Areas A and B in **(b)** are tentatively attributed to aliphatic and aromatic species, respectively.

of organosulfates and nitrooxy-organosulfates in fresh smoke aerosols. For example, laboratory studies have observed the significant formation of organosulfates via photooxidation in the presence of acidic sulfate aerosol (with significant level of SO_2 concentration) (Surratt et al., 2007, 2008). All detected ion species with enabled formula assignments in the present samples are listed in Table S3. In general, CHN and CHS compounds are not ionised well in negative ESI mode, which could be a reason why these species were not the most prevalent compounds in this study.

It should be also noted that the negative ionisation mode selectively targets to detect those molecules containing polar functional groups (e.g. –OH and –COOH) that could be readily deprotonated. There are number of compounds that are not easily deprotonated and might show up preferentially in positive ionisation mode (e.g. amines). Furthermore, the formula numbers detected in the HRMS potentially contain multiple structural isomers; therefore, the actual number of water-soluble organic species is expected to be underestimated. The additional LC/ESI-HRMS analysis operated in negative mode confirmed a substantial number of ion masses (e.g. assigned CHO and CHON compounds) containing more than one structural isomer, which could be observed at different retention times (RTs) in chromatograms. Two representative groups of extracted chromatograms for CHO ($[C_7H_5O_n]^-$, ($n = 2$–4)) and CHON ($[C_7H_5O_nN]^-$, ($n = 1$–3)) compounds are shown in Figs. S3 and S4, respectively, where increasing the O or N atom number in a molecule might lead to more isomer peaks. However, it should be noted that these LC-separated peaks might also include other unidentified compounds that were outside of the elemental assignment considered in this study. Additionally, low mass loading and potential decomposition under the ionisation can also limit the detection of some high molecular-weight species.

The interpretation of the complex organic mass spectra generated by high-resolution mass spectrometry can be simplified by plotting the hydrogen-to-carbon ratio (H/C) against the oxygen-to-carbon ratio (O/C) for individual assigned atomic formulas in form of the Van Krevelen (VK) diagram (e.g. Lin et al., 2012a; Kourtchev et al., 2013). Figure 2b indicates a representative VK diagram of CHO and CHON compounds derived from HNWX-1 sample. It can be clearly seen from Fig. 2b that the majority of CHO and CHON molecules are located in the region of $O/C \leq 1.0$ and $H/C \leq 2.0$. In VK diagram, molecules with $H/C \leq 1.0$ and $O/C \leq 0.5$ are typical for aromatic species, while molecules with $H/C \geq 1.5$ and $O/C \leq 0.5$ would be associated with typical aliphatic compounds (Mazzoleni et al., 2012; Kourtchev et al., 2013). The average DBE showed relatively high values of 5.5 for CHO compounds and 6.1 for CHON compounds (Table S2), suggesting that unsaturated organic species were abundant in the present samples, and their presence could partially account for the strong light-absorbing feature in the near-UV region as observed in our previous study (Cai et al., 2018).

Throughout the extract samples, the average H/C and O/C values ranged from 1.26 ± 0.38 to 1.31 ± 0.40 and from 0.34 ± 0.24 to 0.42 ± 0.29 for CHO compounds and from 1.19 ± 0.32 to 1.23 ± 0.35 and from 0.28 ± 0.17 to 0.29 ± 0.15 for CHON compounds (Table S2), respectively. Although the ESI analysis was performed in the negative ionisation mode, the measured O/C exhibits rather low values, which fall in the range of O/C ratios typical for biomass burning organic aerosol derived from positive ionisation mode (Aiken et al., 2008; Kourtchev et al., 2016). Due to fresh emission and a smaller ageing effect, the present O/C was obviously lower than the O/C of long-range transport biomass burning aerosols (Zhang et al., 2018).

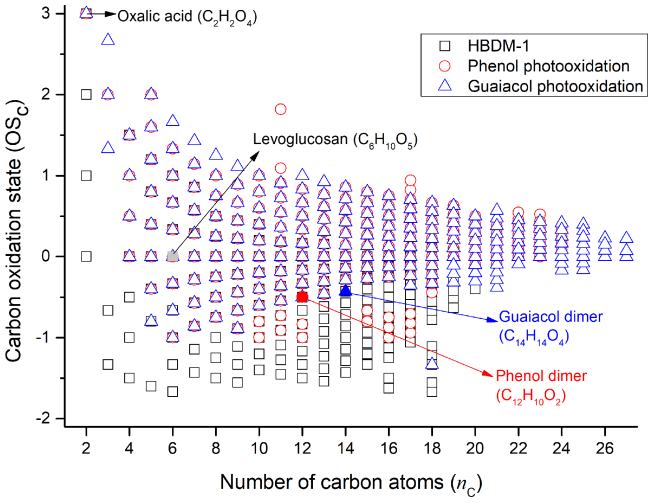

Figure 3. The distribution of carbon oxidation state (OS_C) for CHO molecules in HBDM-1 and laboratory samples produced from phenol and guaiacol photooxidation in the presence of H_2O_2 (i.e. phenol + H_2O_2 and guaiacol + H_2O_2). The locations of oxalic acid (identified in HBDM-1 and laboratory samples), levoglucosan (identified in HBDM-1), phenol dimer (identified in phenol + H_2O_2), and guaiacol dimer (identified in guaiacol + H_2O_2) are shown.

The carbon oxidation state (OS_C) was observed to increase with oxidation for atmospheric organic aerosol and was linked strongly to aerosol volatility (Kroll et al., 2011). OS_C for each molecular formula can be calculated using the following equation:

$$OS_C = -\sum_i OS_i \frac{n_i}{n_C}, \quad (1)$$

where OS_i is the oxidation state associated with the non-carbon element i and n_i/n_C is the molar ratio of element i to carbon within the molecule (Kroll et al., 2011; Kourtchev et al., 2013).

Considering that nitrogen and sulfur atoms can present multiple oxidation states, the OS_C was calculated and analysed only for CHO compounds in this study. A similar pattern of OS_C values versus the number of carbon atoms (n_C) was observed for CHO compounds detected in the present WSBA samples (Figs. 3 and S5). From Figs. 3 and S5, it can be seen that OS_C of each sample ranges mainly from -1.5 to $+1$ with the average ranging from -0.6 to -0.4. Consistent with previous studies (Kroll et al., 2011; Kourtchev et al., 2016), the majority of molecules with $OS_C < 0$ (low oxidised organics) and carbon atoms lower than 20 are suggested to be associated with the primary organic aerosols emitted from biomass burning. A minor fraction of molecular formulas with $OS_C \geq 0$ values might be associated with semivolatile and low-volatility oxidised organic aerosols (Kroll et al., 2011). Figure 3 also shows the plot of OS_C versus n_C for products obtained from the photooxidation of phenol and guaiacol, respectively, and their comparison with WSBA samples will be discussed in Sect. 3.3.

3.2 Mass spectral characteristics of the products from photooxidation of phenolic compounds in the aqueous phase

Phenol and guaiacol were chosen as two representative model compounds derived from biomass combustion. Two high-resolution mass spectra of aqueous phenol and guaiacol exposed to OH radicals for 4 h are shown in Fig. S6, where 435 $C_xH_yO_z$ molecular formulas (m/z 90–500) were assigned for product ions of phenol (with C_3–C_{24}) and 624 $C_xH_yO_z$ formulas (m/z 90–600) were assigned for product ions of guaiacol (with C_3–C_{27}). The average H/C and O/C values were 0.79 ± 0.28 and 0.52 ± 0.23 for phenol, and 0.88 ± 0.24 and 0.59 ± 0.24 for guaiacol, respectively. Clearly, the photochemical processing induced by OH oxidation resulted in an increase in the average O/C of product molecules relative to their precursors (O/C = 0.17 for phenol and O/C = 0.29 for guaiacol).

The formation mechanisms of series of oxygenated products, e.g. phenolic oligomers, hydroxylated phenolic species, and ring-opening and highly oxygenated compounds, are proposed in the literature (e.g. Sun et al., 2010; Chang and Thompson, 2010; Yu et al., 2014). The OH-initiated reactions would result in enhanced hydroxylation of the aromatic ring as well as in increased yields of carboxylic acids and toxic dicarbonyl compounds (Sun et al., 2010; Yu et al., 2014; Prasse et al., 2018). For example, some highly oxygenated C_2–C_5 aliphatic compounds (e.g. $C_2H_2O_4$, $C_3H_4O_4$, $C_4H_6O_4$, and $C_5H_6O_5$) corresponding to carboxylic acids (Yu et al., 2014) were clearly observed in the mass spectra of present photochemical products. The occurrence of these oxygenated products not only directly increased the degree of oxygenation in the bulk solution composition but also contributed to the variation in solution acidity. After the 4 h photochemical process, the pH values of the irradiated solution were significantly lower than the pH values of the solution prior to irradiation (t test, $p < 0.05$), and the calculated acidities ($[H^+]$) of the bulk solution increased by $(2.96 \pm 0.15) \times 10^{-5}$ M and $(4.26 \pm 0.16) \times 10^{-5}$ M for phenol and guaiacol, respectively.

The oligomerisation induced by photochemical transformation of phenolic substances is an important formation pathway for low-volatility, light-absorbing compounds (Smith et al., 2016). Here, phenolic dimmers (i.e. $C_{12}H_{10}O_2$ for phenol dimer and $C_{14}H_{14}O_4$ for guaiacol dimer) and higher oligomers (e.g. $C_{18}H_{14}O_3$ and $C_{24}H_{18}O_4$ for phenol trimer and tetramer, $C_{21}H_{20}O_6$ for guaiacol trimer), as well as their hydroxylated species were observed. The formation mechanism can be ascribed to C–O or C–C coupling of phenoxy radicals that were formed via H abstraction of the phenols or OH addition to the aromatic ring (Net et al., 2009; Sun et al., 2010). The reaction at the para position or para–para coupling was more likely to occur due to a higher probability

of free electrons to occur in this position (Lavi et al., 2017) or a weaker steric hindrance in the para position.

3.3 Comparison of the photochemical products of phenolic compounds and the CHO composition in WSOC extracts from WSBA samples

Compared to the CHO compounds detected in WSOC extracts, the photochemical products of the two phenols under study showed a higher O/C and a lower H/C value. The average OS_C of photochemical products from phenol ($OS_C = -0.7$) and guaiacol ($OS_C = -0.6$) after a 4 h photooxidation rose to $+0.2$ and $+0.3$, respectively, showing distinctly a higher degree of oxidation than the present WSBA samples. In Fig. 3, more species with $OS_C < 0$ (especially $OS_C < -0.5$) are presented in the field sample (HBDM-1), while the species with $OS_C \geq 0$ are prevalent in photochemical products of phenol and guaiacol. The single-precursor systems in laboratory did not completely reflect the CHO composition features in water-soluble extracts from real straw-burning samples that contained a myriad of precursors and unknown substances from atmospheric background, soil, and other sources. Considering that a large number of phenols and methoxyphenols exist in the straw-burning smokes and their potential to undergo photochemical ageing, the nature of emitted primary organic aerosols is reasonably more complicated than the nature of simulated products derived from single-precursor systems.

The extracted LC chromatograms of m/z 185.0608 and 245.0823 are shown in Fig. 4, respectively, where both ions involve dimers of phenol and guaiacol with several structures and/or other isomers. The presence of guaiacol dimer and syringol dimer was previously observed in aerosol samples largely affected by wood combustion. Based on the aerosol mass spectrometer (AMS) analysis, these two dimers were suggested as markers of biomass burning aerosols (Sun et al., 2010; Yu et al., 2014). In the composition of present biomass burning aerosols, the phenolic dimers (m/z 185.0608 and 245.0823) were also observed in the present mass spectra, but the extracted LC chromatograms shown in Fig. 4 indicate that these ions contain multiple RT peaks. The same peaks with RT 18.3 and 19.2 min which are assumed to be the phenol dimers were observed during the photochemical transformation of phenol (Fig. 4a) and in the WSBA samples. Meanwhile, the present particle extracts may also involve guaiacol dimer, since its m/z 245.0823 has two LC peaks emerging at RT 17.7 and 19.5 min (Fig. 4b), the same as the peaks identified during the photochemical transformation of guaiacol. Considering that a substantial amount of moisture in the plant body (Bi et al., 2009) was discharged during the process of straw combustion, the occurrence of phenolic dimers might indicate that the aqueous-phase reactions played an important role in the formation and evolution of emitted aerosol organic composition.

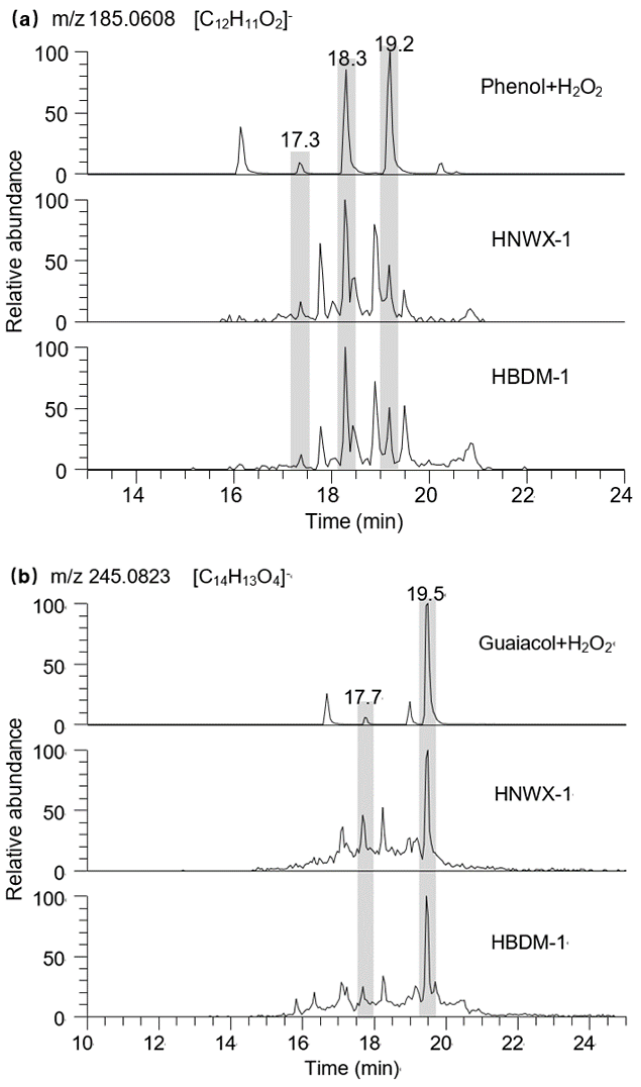

Figure 4. Extracted LC chromatograms of **(a)** m/z 185.0608 and **(b)** m/z 245.0823 in photochemical samples of phenols, HNWX-1, and HBDM-1.

Typical hydroxylated species, such as $C_2H_2O_4$, $C_6H_6O_2$, $C_7H_6O_3$, and $C_7H_8O_3$, were also found in the samples from photooxidation of both phenols and the WSBA samples. The comparison of the photochemical products from phenols and the WSBA samples revealed their significant difference, pointing to the importance of studying real aerosol samples against the laboratory model compounds. However, evaluating the model compounds as a proxy of real aerosol samples is always helpful as a reference. To this end, it is worth noting that potentially other phenols and methoxyphenols (e.g. acetosyringone, vanillin) that dissolve into cloud, fog droplets, or aerosol liquid water can be photochemically transformed and can contribute to SOA formation (Vione et al., 2019; Zhou et al., 2019).

3.4 Photolysis of WSOC extracts from WSBA samples

Although the direct photolysis was performed on present WSOC extracts from WSBA samples in the presence of simulated sunlight irradiation without adding any oxidants, the photooxidation process still occurred since the particle extracts were very likely to include various oxidants, e.g. singlet molecular oxygen ($^1O_2$), peroxides, hydroxyl radical (OH), or an excited triplet state of organics produced under light excitation (Anastasio et al., 1997; Vione et al., 2006; Net et al., 2009, 2010a; Bateman et al., 2011; Rossignol et al., 2014; Smith et al., 2014; Gómez Alvarez et al., 2012). In particular, the excited triplet state of aromatic carbonyls (e.g. 3, 4-dimethoxybenzaldehyde) (Net et al., 2010b) was found to be more efficient than OH radicals to oxidise phenols and produce hydroxylated species (Smith et al., 2014; Yu et al., 2014). This photosensitised reaction is likely to play an important role in the WSOC evolution, due to high quantities of aromatic carbonyls present in the extracts of biomass burning aerosols.

The variation in peak abundance at unique retention times in the chromatogram could reflect the extent of the evolution of WSOC molecules with accurate molecular weights, although no available standards were utilised for absolute quantification. The LC/ESI-HRMS monitors obvious change in the molecular features of partial CHO species, i.e. photodegradation of low oxygenated compounds and formation of highly oxygenated compounds. Table 1 lists the CHO compounds for which the LC peak intensities significantly increased and decreased after the 12 h photolysis.

3.4.1 Photodegradation of low oxygenated compounds and formation of highly oxygenated compounds

As shown in Table 1, ion masses assigned to high unsaturated and low oxygenated species (O/C < 0.5) are prone to photodegradation, especially C_7–C_9 compounds (possible aromatic species), the intensity of which decreased by nearly 1 order of magnitude. For example, for m/z 123.0450 ($[C_7H_7O_2]^-$), as shown in Fig. 5a, the peaks at RT 16.2 and 16.7 min in the LC chromatogram reduced in area by 95 % after the 12 h irradiation. Using a standard it was verified that both peaks did not belong to guaiacol (peak at RT 17.3 min), but they were also found within the products of guaiacol photooxidation, suggesting that they might be isomers of guaiacol or aromatic dihydric alcohol.

The phenolic dimers ($C_{12}H_{10}O_2$ and $C_{14}H_{14}O_4$) as described above also exhibited a decreasing tendency, with an almost complete disappearance after 12 h direct photolysis. Other species with relatively high molecular weight (MW) ($\geq$ 200 Da) were also observed to be decomposed, including m/z 251.0564 ($[C_{12}H_{11}O_6]^-$), 313.0724 ($[C_{17}H_{13}O_6]^-$), and 329.0674 ($[C_{17}H_{13}O_7]^-$) (Fig. S7), although their initial abundance was not very high.

On the other hand, the solution acidity ($[H^+]$) of the particle extracts increase after the 12 h photolysis, similar to the observation on the photooxidation of phenols (Sect. 3.2) that resulted in the formation of oxygenated species. The solution acidity ($[H^+]$) normalised by WSOC concentration ($[OC_{ws}]$) was increased with a variation in $\Delta[H^+]/[OC_{ws}] = (3.8 \pm 0.8) \times 10^{-7}$ mol mg C^{-1}, suggesting the formation of new acidic substances.

The photochemical processing led to an increased formation of low MW compounds (e.g. C_2–C_5 species), with a relatively high O/C. For example, the C_2 compounds, including $[C_2H_1O_3]^-$, $[C_2H_3O_3]^-$, $[C_2H_3O_2]^-$, and $[C_2H_1O_4]^-$ (Fig. S8), which may correspond to glyoxylic acid, glycolic acid, acetic acid, and oxalic acid, respectively, were likely to be formed via the oxidation pathway of several water-soluble molecules with photochemical reactivity, e.g. glyoxal (Carlton et al., 2007; Lim et al., 2010), methylglyoxal (Altieri et al., 2008; Lim et al., 2010), pyruvic acid (e.g. Grgic et al., 2010; Griffith et al., 2013; Reed Harris et al., 2014; Rapf et al., 2017; Eugene and Guzman, 2017; Mekic et al., 2018, 2019), and phenols (Sun et al., 2010). The presence of these highly oxygenated compounds that possibly contain acidic groups (e.g. –COOH and –OH) undoubtedly contributed to the increase in the solution acidity. Higher levels of other highly oxygenated species such as $[C_3H_5O_3]^-$, $[C_4H_7O_2]^-$, $[C_5H_5O_5]^-$, and $[C_5H_7O_5]^-$ were also observed (Fig. S9).

To identify the impact of photolysis on the evolution of specific WSOC, the ions of $[C_7H_7O_n]^-$ in the HBDM-1 sample with significant variation were chosen as representative cases for description. The relative intensity of $[C_7H_7O_2]^-$ and $[C_7H_7O_3]^-$ decreased dramatically, while the intensities of $[C_7H_7O_4]^-$, $[C_7H_7O_5]^-$, and $[C_7H_7O_6]^-$ increased with the irradiation time (Fig. 5 shows only the variation in $[C_7H_7O_2]^-$ and $[C_7H_7O_4]^-$ as an example). It seems reasonable that the possible hydroxylation of $[C_7H_7O_2]^-$ and $[C_7H_7O_3]^-$ might contribute to the formation of $[C_7H_7O_5]^-$ and $[C_7H_7O_6]^-$. Although we could not verify this hypothesis, the oxidised species formed undoubtedly have a high O/C, which highlights the possibility of this reaction pathway.

3.4.2 Presentation of photochemically stable organic species

Some of the detected organic species seemed to exhibit a good photochemical stability, as their relative intensities only slightly decreased (< 10 %) after 12 h light irradiation. The m/z 161.0454 ($[C_6H_9O_5]^-$) presented two prominent peaks at RT 1.9 and 2.4 min (Fig. S10). The peak at RT 2.4 min was further confirmed with a standard compound to be levoglucosan, a typical tracer of biomass burning aerosols with a high photochemical stability in atmospheric aerosols (Hu et al., 2013). The relatively good photochemical stability was also observed for some C_6 homologue compounds, such as $[C_6H_7O_6]^-$, $[C_6H_9O_6]^-$, and $[C_6H_{11}O_6]^-$. Some

Table 1. m/z with significant changes upon 12 h photolysis analysed by LC/ESI-HRMS.

Precursor (LC peak intensity decreases by > 50 %)			Product (LC peak intensity increases by > 50 %)		
Retention time, minutes	Measured m/z	Molecular formula	Retention time, minutes	Measured m/z	Molecular formula
16.2, 16.7	123.04497	$C_7H_8O_2$	1.9	59.01362	$C_2H_4O_2$
13.9, 14.5	129.05555	$C_6H_{10}O_3$	1.8	72.99291	$C_2H_2O_3$
14.6	131.07121	$C_6H_{12}O_3$	2.1	73.02928	$C_3H_6O_2$
14.6	133.02934	$C_8H_6O_2$	1.8	75.00856	$C_2H_4O_3$
15.9	135.04498	$C_8H_8O_2$	2.4	85.02930	$C_4H_6O_2$
13.7	137.02426	$C_7H_6O_3$	1.9, 4.4	87.04496	$C_4H_8O_2$
17.7	137.06063	$C_8H_{10}O_2$	1.9	88.98785	$C_2H_2O_4$
15.8	147.04504	$C_9H_8O_2$	1.9	89.02427	$C_3H_6O_3$
17.2	149.06062	$C_9H_{10}O_2$	2.2	99.00857	$C_4H_4O_3$
19.0	151.07634	$C_9H_{12}O_2$	2.5	129.01917	$C_5H_6O_4$
16.8	161.06068	$C_{10}H_{10}O_2$	2.0	145.01407	$C_5H_6O_5$
16.2	165.05559	$C_9H_{10}O_3$	1.9	147.02971	$C_5H_8O_5$
14.9	167.07129	$C_9H_{12}O_3$	14.9	155.03482	$C_7H_8O_4$
15.1	181.05048	$C_9H_{10}O_4$	15.1	169.01411	$C_7H_6O_5$
17.3	191.03498	$C_{10}H_8O_4$	16.4	183.02980	$C_8H_8O_5$
16.2	195.06622	$C_{10}H_{12}O_4$			
18.6	207.06635	$C_{11}H_{12}O_4$			
18.6	329.06742	$C_{17}H_{14}O_7$			

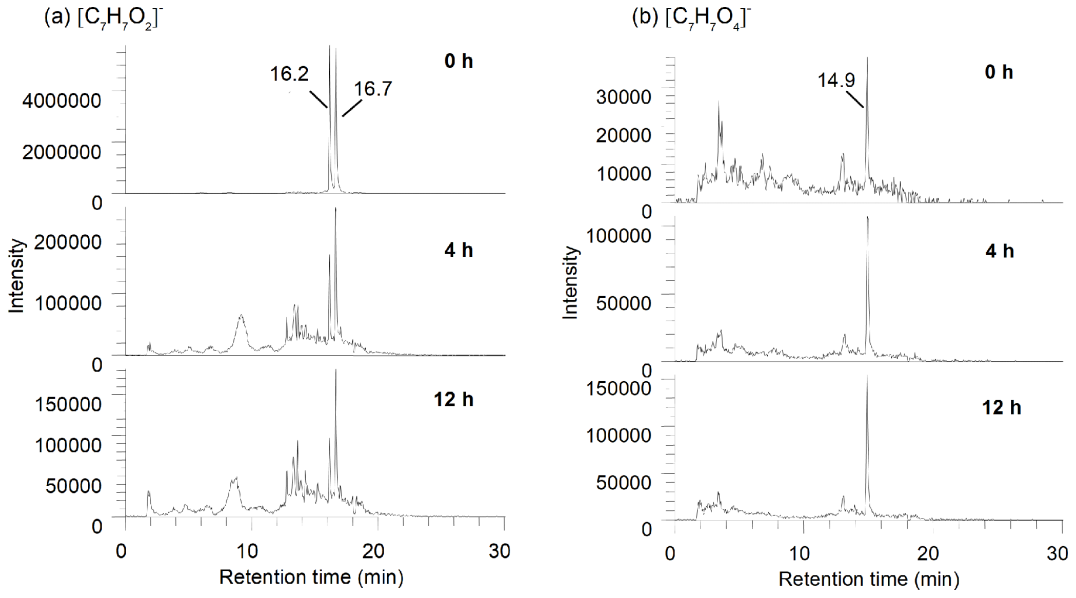

Figure 5. Extracted LC chromatograms from HBDM-1 of **(a)** $[C_7H_7O_2]^-$ and **(b)** $[C_7H_7O_4]^-$ at different photolytic stages of 0, 4, and 12 h.

other oxygenated species, such as $[C_3H_3O_3]^-$, $[C_4H_5O_4]^-$, $[C_3H_3O_4]^-$, and $[C_4H_5O_5]^-$, remained relatively stable as well.

Regarding the CHON compounds, only a small variation in the chromatogram peaks was observed for most of the detected species. In particular, several species with a low O/C decreased by less than 30 %, e.g. m/z 94.0297 ($[C_5H_4ON]^-$, RT 7.1 min) and 120.0453 ($[C_7H_6ON]^-$, RT 12.2 min). Some compounds seem photochemically very stable as the variation in their peak intensities was less than 10 % upon light irradiation of the samples, e.g. m/z 118.0297 ($[C_7H_4ON]^-$, RT 16.6 and 17.1 min), 146.0246 ($[C_8H_4O_2N]^-$, RT 14.4 min), and 190.0510 ($[C_{10}H_8O_3N]^-$, RT 17.8 min). However, the intensities of the ion masses with a relatively higher degree of oxygenation were found to increase substantially

(> 50 %), e.g. m/z 162.0195 ($[C_8H_4O_3N]^-$, RT 17.2 min), 198.0408 ($[C_8H_8O_5N]^-$, RT 18.0 min), and 242.1763 ($[C_{13}H_{24}O_3N]^-$, RT 17.9 min). The photochemical stability of some compounds may be ascribed to their low concentrations, or the light-shielding effect from other light-absorbing species.

Another intriguing finding was that different structural isomers with the same molecular mass might have exhibited different fates upon prolonged light irradiation of the samples. For example, the intensity of the peak at m/z 165.0405 ($[C_5H_9O_6]^-$) decreased when it was eluted at 4.9 min, but increased at RT 1.8 min, with the irradiation time (Fig. S11). A simultaneous degradation and formation among isomers of some CHON ion masses upon prolonged light irradiation was also observed, as was the case for the CHO compounds. For example, the m/z 108.0453 assigned to $[C_6H_6ON]^-$, might include hydroxy and amino groups on the phenyl ring to present three possible isomers (Fig. S12). During photolytic processing, the intensity of the peak at RT 3.2 min increased dramatically, while there was a clear decreasing tendency of the peak intensity at RT 5.5 and 12.5 min, which was suggestive of possible isomerisation among these isomers. Other ion masses that exhibited possible isomerisation included m/z 122.0610 ($[C_7H_8ON]^-$), 132.0454 ($[C_8H_6ON]^-$), 134.0245 ($[C_7H_4O_2N]^-$), 136.0403 ($[C_7H_6O_2N]^-$), 138.0559 ($[C_7H_8O_2N]^-$), 144.0453 ($[C_9H_6ON]^-$), and 152.0352 ($[C_7H_6O_3N]^-$).

3.4.3 Comparison of time-profile mass spectra of CHO composition in WSOC extracts from WSBA samples

Since the LC method just separated a fraction of polar compounds, we tentatively utilised the change in HRMS to gain more comprehensive information about the WSOC evolution. We compared the time-profile (0, 4, and 12 h) mass spectra with each other, based on the assumption of the same interference from inorganic species, and the good reproducibility and stability for Orbitrap MS operated under the same instrumental parameters (the RSD of TIC intensity within 5 %). It is well known that ESI mass spectral abundances are influenced by the solution composition, concentration of analytes, and instrumental factors (Bateman et al., 2011); hence, it is quite challenging to directly quantify the absolute concentration levels of the complex mixtures. Despite this, the photochemical degradation of WSOC compounds and corresponding formation of organic compounds can be well described by the variation in signal intensity from mass spectrometry. The average O/C and H/C for CHO compounds ranged from 0.38 ± 0.02 to 0.44 ± 0.02 and 1.24 ± 0.03 to 1.26 ± 0.01, respectively, as the irradiation time extended from 0 to 12 h. The comparison of these time-profile mass spectra indicates that the 12 h photolysis resulted in a significant reduction in 28 ± 11 % in the total ion abundance (S/N). Since the photolysis induced changes in abundance for most of the CHO compounds, we also calculated the intensity (S/N)-weighted average O/C (O/C_w) and H/C (H/C_w) (Bateman et al., 2011; Romonosky et al., 2015) with values ranging from 0.45 ± 0.03 to 0.53 ± 0.06 and from 1.32 ± 0.09 to 1.40 ± 0.11, respectively. After the 12 h photolysis, both average H/C and H/C_w values slightly increased, compared to the samples prior to irradiation; however, both average O/C and O/C_w values have increased more distinctly, indicating an elevation in oxidation degree of bulk extract composition. This phenomenon could be partly reflected in the LC-HRMS observation, i.e. the formation of highly oxygenated species and the consumption of low oxygenated compounds. In our previous study, the UV–vis measurements revealed that the 12 h photochemical evolution leads to a modification of absorptive properties for WSBA extracts (e.g. photo-bleaching at wavelengths below 380 nm and photo-enhancement above 380 nm) (Cai et al., 2018), which might be partially linked to the present findings about molecular functionalisation, e.g. hydroxylation facilitating a red shift for light-absorbing wavelengths.

4 Conclusions

This study was focused on the effect of direct photolysis on the molecular composition of actual WSOC extracted from field straw-burning aerosol. The phenol dimer (m/z 185.0608) and guaiacol dimer (m/z 245.0823), or their isomers generated from laboratory aqueous-phase photooxidation of phenol and guaiacol, were also observed in the present field WSBA samples, suggesting that the aqueous-phase reaction might contribute to the formation of emitted biomass burning aerosols. The laboratory observation on the aqueous photochemistry of phenols indicated that those phenolic compounds in real biomass burning aerosols would likely have the potential to experience a similar evolution to form various oxygenated compounds under the relevant atmospheric water conditions. The direct photolysis of the molecular composition of WSOC extracts from WSBA samples was performed to gain more insight into the evolution of aerosol composition. Because the extract composition was very complex, the techniques (ESI-HRMS and LC/ESI-HRMS) used in this study, although advanced, still had limitations in monitoring the modification of molecular composition, especially for determining the potential formation of compounds present at low concentrations or compounds that were poorly ionised. However, a series of polar molecules were identified that changed their molecular composition via photochemical ageing. In particular, the degradation of low oxygenated compounds with strong photochemical reactivity and the formation of highly oxygenated compounds might directly result in an increasing O/C in WSOC composition, which was likely linked to the modification of light-absorbing characteristics for extracts in previous study. This

finding indicates that the water-soluble organic fraction of field combustion-derived aerosols has the potential to form more oxidised organic matter, which might contribute to the highly oxygenated nature of atmospheric organic aerosols. Further studies focused on the photochemical evolution of WSOC composition will be performed in the future, including enlarging measurements on compound species (e.g. applying positive ESI-HRMS), identifying biomarkers, and evaluating their role in photochemical processes.

Data availability. The data used in this study are available from the corresponding author on request.

Supplement. The supplement related to this article is available online at: https://doi.org/10.5194/acp-20-6115-2020-supplement.

Author contributions. JC and ZY designed the experiments, and JC and XZ carried them out. GZ provided the straw-burning aerosol samples; ZY and SG helped to perform the analysis of light irradiation and to edit the paper. GS, XW, and PP provided some technical consultations about organic chemistry. JC prepared the paper with contributions from all co-authors.

Competing interests. The authors declare that they have no conflict of interest.

Acknowledgements. The authors acknowledge support provided by the State Key Laboratory of Organic Geochemistry in Guangzhou Institute of Geochemistry, the Chinese Academy of Sciences (GIGCAS), and the Guangdong Key Laboratory of Environment and Resources. This is contribution no. IS-2560 from GIGCAS.

Financial support. This research has been financially supported by the National Key Technology Research and Development Program of the Ministry of Science and Technology of China (grant no. 2014BAC22B04), and the National Natural Science Foundations of China (grant nos. 41225013, 41530641, 41373131, 41773131, and 41977187). We are also supported by the Guangdong Foundation for the Program of Science and Technology Research (grant no. 2017B030314057).

Review statement. This paper was edited by Neil M. Donahue and reviewed by three anonymous referees.

References

Aiken, A. C., Decarlo, P. F., Kroll, J. H., Worsnop, D. R., Alex Huffman, J., Docherty, K. S., Ulbrich, I. M., Mohr, C., Kimmel, J. R., Sueper, D., Sun, Y., Zhang, Q., Trimborn, A., Northway, M., Ziemann, P. J., Canagaratna, M. R., Onasch, T. B., Rami Alfarra, M., Prevot, A. S. H., Dommen, J., Duplissy, J., Metzger, A., Baltensperger, U., and Jimenez, J. L.: O/C and OM/OC Ratios of primary, secondary, and ambient organic aerosols with high-resolution time-of-flight aerosol mass spectrometry, Environ. Sci. Technol., 42, 4478–4485, https://doi.org/10.1021/es703009q, 2008.

Altieri, K. E., Seitzinger, S. P., Carlton, A. G., Turpin, B. J., Klein, G. C., and Marshall, A. G.: Oligomers formed through in-cloud methylglyoxal reactions: Chemical composition, properties, and mechanisms investigated by ultra-high resolution FT-ICR mass spectrometry, Atmos. Environ., 42, 1476–1490, 2008.

Altieri, K. E., Turpin, B. J., and Seitzinger, S. P.: Oligomers, organosulfates, and nitrooxy organosulfates in rainwater identified by ultra-high resolution electrospray ionization FT-ICR mass spectrometry, Atmos. Chem. Phys., 9, 2533–2542, https://doi.org/10.5194/acp-9-2533-2009, 2009a.

Altieri, K. E., Turpin, B. J., and Seitzinger, S. P.: Composition of Dissolved Organic Nitrogen in Continental Precipitation Investigated by Ultra-High Resolution FT-ICR Mass Spectrometry, Environ. Sci. Technol., 43, 6950–6955, https://doi.org/10.1021/es9007849, 2009b.

Anastasio, C., Faust, B. C., and Rao, C. J.: Aromatic carbonyl compounds as aqueous-phase photochemical sources of hydrogen peroxide in acidic sulfate aerosols, fogs, and clouds. 1. Non-phenolic methoxybenzaldehydes and methoxyacetophenones with reductants (phenols), Environ. Sci. Technol., 31, 218–232, 1997.

Bateman, A. P., Nizkorodov, S. A., Laskin, J., and Laskin, A.: Photolytic processing of secondary organic aerosols dissolved in cloud droplets, Phys. Chem. Chem. Phys., 13, 12199–12212, https://doi.org/10.1039/c1cp20526a, 2011.

Bi, Y., Gao, C., Wang, Y., and Li, B.: Estimation of straw resources in China, Transactions of the Chinese Society of Agricultural Engineering, 25, 211–217, 2009.

Boone, E. J., Laskin, A., Laskin, J., Wirth, C., Shepson, P. B., Stirm, B. H., and Pratt, K. A.: Aqueous Processing of Atmospheric Organic Particles in Cloud Water Collected via Aircraft Sampling, Environ. Sci. Technol., 49, 8523–8530, https://doi.org/10.1021/acs.est.5b01639, 2015.

Cai, J., Zhi, G., Yu, Z., Nie, P., Gligorovski, S., Zhang, Y., Zhu, L., Guo, X., Li, P., He, T., He, Y., Sun, J., and Zhang, Y.: Spectral changes induced by pH variation of aqueous extracts derived from biomass burning aerosols: Under dark and in presence of simulated sunlight irradiation, Atmos. Environ., 185, 1–6, https://doi.org/10.1016/j.atmosenv.2018.04.037, 2018.

Cappiello, A., De Simoni, E., Fiorucci, C., Mangani, F., Palma, P., Trufelli, H., Decesari, S., Facchini, M. C., and Fuzzi, S.: Molecular characterization of the water-soluble organic compounds in fogwater by ESIMS/MS, Environ. Sci. Technol., 37, 1229–1240, https://doi.org/10.1021/es0259990, 2003.

Carlton, A. G., Turpin, B. J., Altieri, K. E., Seitzinger, S., Reff, A., Lim, H.-J., and Ervens, B.: Atmospheric oxalic acid and SOA production from glyoxal: Results of aqueous photooxidation experiments, Atmos. Environ., 41, 7588–7602, 2007.

Chang, J. L. and Thompson, J. E.: Characterization of colored products formed during irradiation of aqueous solutions containing H_2O_2 and phenolic compounds, Atmos. Environ., 44, 541–551, https://doi.org/10.1016/j.atmosenv.2009.10.042, 2010.

Collett, J. L., Hoag, K. J., Sherman, D. E., Bator, A., and Richards, W. L.: Spatial and temporal variations in San Joaquin Valley fog chemistry, Atmos. Environ., 33, 129–140, 1998.

Daumit, K. E., Carrasquillo, A. J., Hunter, J. F., and Kroll, J. H.: Laboratory studies of the aqueous-phase oxidation of polyols: submicron particles vs. bulk aqueous solution, Atmos. Chem. Phys., 14, 10773–10784, https://doi.org/10.5194/acp-14-10773-2014, 2014.

Duarte, R. M. B. O., Santos, E. B. H., Pio, C. A., and Duarte, A. C.: Comparison of structural features of water-soluble organic matter from atmospheric aerosols with those of aquatic humic substances, Atmos. Environ., 41, 8100–8113, https://doi.org/10.1016/j.atmosenv.2007.06.034, 2007.

Eugene, A. J. and Guzman, M. I.: Reactivity of Ketyl and Acetyl Radicals from Direct Solar Actinic Photolysis of Aqueous Pyruvic Acid, J. Phys. Chem. A, 121, 2924–2935, 2017.

Fahey, K. M., Pandis, S. N., Collett, J. L., and Herckes, P.: The influence of size-dependent droplet composition on pollutant processing by fogs, Atmos. Environ., 39, 4561–4574, 2005.

Fine, P. M., Cass, G. R., and Simoneit, B. R. T.: Chemical characterization of fine particle emissions from fireplace combustion of woods grown in the northeastern United States, Environ. Sci. Technol., 35, 2665–2675, 2001.

Fu, P. Q., Kawamura, K., Chen, J., Qin, M. Y., Ren, L. J., Sun, Y. L., Wang, Z. F., Barrie, L. A., Tachibana, E., Ding, A. J., and Yamashita, Y.: Fluorescent water-soluble organic aerosols in the High Arctic atmosphere, Sci. Rep.-UK, 5, 9845, https://doi.org/10.1038/srep09845, 2015.

Gilardoni, S., Massoli, P., Paglione, M., Giulianelli, L., Carbone, C., Rinaldi, M., Decesari, S., Sandrini, S., Costabile, F., Gobbi, G. P., Pietrogrande, M. C., Visentin, M., Scotto, F., Fuzzi, S., and Facchini, M. C.: Direct observation of aqueous secondary organic aerosol from biomass-burning emissions, P. Natl. Acad. Sci. USA, 113, 10013–10018, 2016.

Gómez Alvarez, E., Wortham, H., Strekowski, R., Zetzsch, C., and Gligorovski, S.: Atmospheric photo-sensitized heterogeneous and multiphase reactions: From outdoors to indoors, Environ. Sci. Technol., 46, 1955–1963, 2012.

Graham, B., Mayol-Bracero, O. L., Guyon, P., Roberts, G. C., Decesari, S., Facchini, M. C., Artaxo, P., Maenhaut, W., Koll, P., and Andreae, M. O.: Water-soluble organic compounds in biomass burning aerosols over Amazonia-1. Characterization by NMR and GC-MS, J. Geophys. Res.-Atmos., 107, LBA 14-1–LBA 14-16, https://doi.org/10.1029/2001jd000336, 2002.

Grgic, I., Nieto-Gligorovski, L. I., Net, S., Temime-Roussel, B., Gligorovski, S., and Wortham, H.: Light induced multiphase chemistry of gas-phase ozone on aqueous pyruvic and oxalic acids, Phys. Chem. Chem. Phys., 12, 698–707, 2010.

Griffith, E. C., Carpenter, B. K., Shoemaker, R. K., and Vaida, V.: Photochemistry of aqueous pyruvic acid, P. Natl. Acad. Sci. USA, 110, 11714–11719, https://doi.org/10.1073/pnas.1303206110, 2013.

Haynes, J. P., Miller, K. E., and Majestic, B. J.: Investigation into Photoinduced Auto-Oxidation of Polycyclic Aromatic Hydrocarbons Resulting in Brown Carbon Production, Environ. Sci. Technol., 53, 682–691, https://doi.org/10.1021/acs.est.8b05704, 2019.

Hu, Q., Xie, Z., Wang, X., Hui Kang, H., and Zhang, P.: Levoglucosan indicates high levels of biomass burning aerosols over oceans from the Arctic to Antarctic, Sci. Rep.-UK, 3, 3119, https://doi.org/10.1038/srep03119, 2013.

Kitanovski, Z., Čusak, A., Grgić, I., and Claeys, M.: Chemical characterization of the main products formed through aqueous-phase photonitration of guaiacol, Atmos. Meas. Tech., 7, 2457–2470, https://doi.org/10.5194/amt-7-2457-2014, 2014.

Kourtchev, I., Fuller, S., Aalto, J., Ruuskanen, T. M., McLeod, M. W., Maenhaut, W., Jones, R., Kulmala, M., and Kalberer, M.: Molecular Composition of Boreal Forest Aerosol from Hyytiala, Finland, Using Ultrahigh Resolution Mass Spectrometry, Environ. Sci. Technol., 47, 4069–4079, https://doi.org/10.1021/es3051636, 2013.

Kourtchev, I., Godoi, R. H. M., Connors, S., Levine, J. G., Archibald, A. T., Godoi, A. F. L., Paralovo, S. L., Barbosa, C. G. G., Souza, R. A. F., Manzi, A. O., Seco, R., Sjostedt, S., Park, J.-H., Guenther, A., Kim, S., Smith, J., Martin, S. T., and Kalberer, M.: Molecular composition of organic aerosols in central Amazonia: an ultra-high-resolution mass spectrometry study, Atmos. Chem. Phys., 16, 11899–11913, https://doi.org/10.5194/acp-16-11899-2016, 2016.

Krivacsy, Z., Hoffer, A., Sarvari, Z., Temesi, D., Baltensperger, U., Nyeki, S., Weingartner, E., Kleefeld, S., and Jennings, S. G.: Role of organic and black carbon in the chemical composition of atmospheric aerosol at European background sites, Atmos. Environ., 35, 6231–6244, 2001.

Kroll, J. H., Donahue, N. M., Jimenez, J. L., Kessler, S. H., Canagaratna, M. R., Wilson, K. R., Altieri, K. E., Mazzoleni, L. R., Wozniak, A. S., Bluhm, H., Mysak, E. R., Smith, J. D., Kolb,C. E., and Worsnop, D. R.: Carbon oxidation state as a metricfor describing the chemistry of atmospheric organic aerosol, Nat. Chem. Biol., 3, 133–139, 2011.

Laskin, A., Smith, J. S., and Laskin, J.: Molecular Characterization of Nitrogen-Containing Organic Compounds in Biomass Burning Aerosols Using High-Resolution Mass Spectrometry, Environ. Sci. Technol., 43, 3764–3771, https://doi.org/10.1021/es803456n, 2009.

Lavi, A., Lin, P., Bhaduri, B., Carmieli, R., Laskin, A., and Rudich, Y.: Characterization of light-absorbing oligomers from reactions of phenolic compounds and Fe(III), Earth Space Chem., 1, 637–646, 2017.

Lee, A. K. Y., Herckes, P., Leaitch, W. R., Macdonald, A. M., and Abbatt, J. P. D.: Aqueous OH oxidation of ambient organic aerosol and cloud water organics: Formation of highly oxidized products, Geophys. Res. Lett., 38, L11805, https://doi.org/10.1029/2011GL047439, 2011.

Li, J., Wang, X., Chen, J., Zhu, C., Li, W., Li, C., Liu, L., Xu, C., Wen, L., Xue, L., Wang, W., Ding, A., and Herrmann, H.: Chemical composition and droplet size distribution of cloud at the summit of Mount Tai, China, Atmos. Chem. Phys., 17, 9885–9896, https://doi.org/10.5194/acp-17-9885-2017, 2017.

Lim, Y. B. and Turpin, B. J.: Laboratory evidence of organic peroxide and peroxyhemiacetal formation in the aqueous phase and implications for aqueous OH, Atmos. Chem. Phys., 15, 12867–12877, https://doi.org/10.5194/acp-15-12867-2015, 2015.

Lim, Y. B., Tan, Y., Perri, M. J., Seitzinger, S. P., and Turpin, B. J.: Aqueous chemistry and its role in secondary organic aerosol (SOA) formation, Atmos. Chem. Phys., 10, 10521–10539, https://doi.org/10.5194/acp-10-10521-2010, 2010.

Lin, P., Rincon, A. G., Kalberer, M., and Yu, J. Z.: Elemental Composition of HULIS in the Pearl River Delta Region, China: Results Inferred from Positive and Negative Electrospray High Resolution Mass Spectrometric Data, Environ. Sci. Technol., 46, 7454–7462, https://doi.org/10.1021/es300285d, 2012a.

Lin, P., Yu, J. Z., Engling, G., and Kalberer, M.: Organosulfates in Humic-like Substance Fraction Isolated from Aerosols at Seven Locations in East Asia: A Study by Ultra-High-Resolution Mass Spectrometry, Environ. Sci. Technol., 46, 13118–13127, https://doi.org/10.1021/es303570v, 2012b.

Mayol-Bracero, O. L., Guyon, P., Graham, B., Roberts, G., Andreae, M. O., Decesari, S., Facchini, M. C., Fuzzi, S., and Artaxo, P.: Water-soluble organic compounds in biomass burning aerosols over Amazonia – 2. Apportionment of the chemical composition and importance of the polyacidic fraction, J. Geophys. Res.-Atmos., 107, LBA 59-1–LBA 59-15, https://doi.org/10.1029/2001jd000522, 2002.

Mazzoleni, L. R., Saranjampour, P., Dalbec, M. M., Samburova, V., Hallar, A. G., Zielinska, B., Lowenthal, D. H., and Kohl, S.: Identification of water-soluble organic carbon in non-urban aerosols using ultrahigh-resolution FT-ICR mass spectrometry: organic anions, Environ. Chem., 9, 285–297, https://doi.org/10.1071/EN11167, 2012.

McNeill, V. F.: Aqueous Organic Chemistry in the Atmosphere: Sources and Chemical Processing of Organic Aerosols, Environ. Sci. Technol., 49, 1237–1244, 2015.

Mekic, M., Loisel, G., Zhou, W., Jiang, B., Vione, D., and Gligorovski, S.: Ionic strength effects on the reactive uptake of ozone on aqueous pyruvic acid: Implications for air-sea ozone deposition, Environ. Sci. Technol., 52, 12306–12315, 2018.

Mekic, M., Liu, J., Zhou, W., Loisel, G., Cai, J., He, T., Jiang, B., Yu, Z., Lazarou, Y. G., Li, X., Brigante, M., Vione, D., and Gligorovski, S.: Formation of highly oxygenated multifunctional compounds from cross-reactions of carbonyl compounds in the atmospheric aqueous phase, Atmos. Environ., 219, 117046, https://doi.org/10.1016/j.atmosenv.2019.117046, 2019.

Net, S., Nieto-Gligorovski, L., Gligorovski, S., Temime-Rousell, B., Barbati, S., Lazarou, Y. G., and Wortham, H.: Heterogeneous light induced ozone processing on the organic coatings in the atmosphere, Atmos. Environ., 43, 1683–1692, 2009.

Net, S., Nieto-Gligorovski, L., Gligorovski, S., and Wortham, H.: Heterogeneous ozonation kinetics of 4-phenoxyphenol in the presence of photosensitizer, Atmos. Chem. Phys., 10, 1545–1554, https://doi.org/10.5194/acp-10-1545-2010, 2010b.

Net, S., Gligorovski, S., and Wortham, H.: Light-induced heterogeneous ozone processing on organic coated particles: Kinetics and condensed-phase products, Atmos. Environ., 44, 3286–3294, 2010b.

Nguyen, T. B., Lee, P. B., Updyke, K. M., Bones, D. L., Laskin, J., Laskin, A., and Nizkorodov, S. A.: Formation of nitrogen- and sulfur-containing light-absorbing compounds accelerated by evaporation of water from secondary organic aerosols, J. Geophys. Res.-Atmos., 117, D01207, https://doi.org/10.1029/2011jd016944, 2012.

Ofner, J., Krüger, H.-U., Grothe, H., Schmitt-Kopplin, P., Whitmore, K., and Zetzsch, C.: Physico-chemical characterization of SOA derived from catechol and guaiacol – a model substance for the aromatic fraction of atmospheric HULIS, Atmos. Chem. Phys., 11, 1–15, https://doi.org/10.5194/acp-11-1-2011, 2011.

Prasse, C., Ford, B., Nomura, D. K., and Sedlak, D. L.: Unexpected transformation of dissolved phenols to toxic dicarbonyls by hydroxyl radicals and UV light, P. Natl. Acad. Sci. USA, 115, 2311–2316, https://doi.org/10.1073/pnas.1715821115, 2018.

Rapf, R. J., Perkins, R. J., Carpenter, B. K., and Vaida, V.: Mechanistic Description of Photochemical Oligomer Formation from Aqueous Pyruvic Acid, J. Phys. Chem. A, 121, 4272–4282, 2017.

Reed Harris, A. E., Ervens, B., Shoemaker, R. K., Kroll, J. A., Rapf, R. J., Griffith, E. C., Monod, A., and Vaida, V.: Photochemical kinetics of pyruvic acid in aqueous solution, J. Phys. Chem. A, 118, 8505–8516, 2014.

Romonosky, D. E., Laskin, A., Laskin, J., and Nizkorodov, S. A.: High-Resolution Mass Spectrometry and Molecular Characterization of Aqueous Photochemistry Products of Common Types of Secondary Organic Aerosols, J. Phys. Chem. A, 119, 2594–2606, https://doi.org/10.1021/jp509476r, 2015.

Rossignol, S., Aregahegn, K. Z., Tinel, L., Fine, L., Noziere, B., and George, C.: Glyoxal Induced Atmospheric Photosensitized Chemistry Leading to Organic Aerosol Growth, Environ. Sci. Technol., 48, 3218–3227, 2014.

Simoneit, B. R. T.: Biomass burning – A review of organic tracers for smoke from incomplete combustion, Appl. Geochem., 17, 129–162, https://doi.org/10.1016/s0883-2927(01)00061-0, 2002.

Smith, J. D., Sio, V., Yu, L., Zhang, Q., and Anastasio, C.: Secondary Organic Aerosol Production from Aqueous Reactions of Atmospheric Phenols with an Organic Triplet Excited State, Environ. Sci. Technol., 48, 1049–1057, https://doi.org/10.1021/es4045715, 2014.

Smith, J. D., Kinney, H., and Anastasio, C.: Phenolic carbonyls undergo rapid aqueous photodegradation to form low-volatility, light-absorbing products, Atmos. Environ., 126, 36–44, https://doi.org/10.1016/j.atmosenv.2015.11.035, 2016.

Smith, J. S., Laskin, A., and Laskin, J.: Molecular Characterization of Biomass Burning Aerosols Using High-Resolution Mass Spectrometry, Anal. Chem., 81, 1512–1521, https://doi.org/10.1021/ac8020664, 2009.

Sun, Y. L., Zhang, Q., Anastasio, C., and Sun, J.: Insights into secondary organic aerosol formed via aqueous-phase reactions of phenolic compounds based on high resolution mass spectrometry, Atmos. Chem. Phys., 10, 4809–4822, https://doi.org/10.5194/acp-10-4809-2010, 2010.

Surratt, J. D., Kroll, J. H., Kleindienst, T. E., Edney, E. O., Claeys, M., Sorooshian, A., Ng, N. L., Offenberg, J. H., Lewandowski, M., Jaoui, M., Flagan, R. C., and Seinfeld, J. H.: Evidence for organosulfates in secondary organic aerosol, Environ. Sci. Technol., 41, 517–527, https://doi.org/10.1021/es062081q, 2007.

Surratt, J. D., Gomez-Gonzalez, Y., Chan, A. W. H., Vermeylen, R., Shahgholi, M., Kleindienst, T. E., Edney, E. O., Offenberg, J. H., Lewandowski, M., Jaoui, M., Maenhaut, W., Claeys, M., Flagan, R. C., and Seinfeld, J. H.: Organosulfate formation in biogenic secondary organic aerosol, J. Phys. Chem. A, 112, 8345–8378, https://doi.org/10.1021/jp802310p, 2008.

Tong, H., Kourtchev, I., Pant, P., Keyte, I. J., O'Connor, I. P., Wenger, J. C., Pope, F. D., Harrison, R. M., and Kalberer, M.: Molecular composition of organic aerosols at urban background and road tunnel sites using ultra-high resolution mass spectrometry, Faraday Discuss., 189, 51–68, 2016.

Vione, D., Maurino, V., Minero, C., Pelizzetti, E., Harrison, M. A. J., Olariu, R. I., and Arsene, C.: Photochemical reactions in the tropospheric aqueous phase and on particulate matter, Chem. Soc. Rev., 35, 441–453, 2006.

Vione, V., Albinet, A., Barsotti, F., Mekic, M., Jiang, B., Minero, C., Brigante, M., and Gligorovski, S.: Formation of substances with humic-like fluorescence properties, upon photoinduced oligomerization of typical phenolic compounds emitted by biomass burning, Atmos. Environ., 206, 197–207, https://doi.org/10.1016/j.atmosenv.2019.03.005, 2019.

Wang, X., Hayeck, N., Brüggemann, M., Yao, L., Chen, H., Zhang, C., Emmelin, C., Chen, J., George, C., and Wang, L.: Chemical characteristics of organic aerosols in shanghai: A study by ultrahigh-performance liquid chromatography coupled with Orbitrap mass spectrometry, J. Geophys. Res.-Atmos., 122, 703–722, 2017.

Wang, X. K., Rossignol, S., Ma, Y., Yao, L., Wang, M. Y., Chen, J. M., George, C., and Wang, L.: Molecular characterization of atmospheric particulate organosulfates in three megacities at the middle and lower reaches of the Yangtze River, Atmos. Chem. Phys., 16, 2285–2298, https://doi.org/10.5194/acp-16-2285-2016, 2016.

Wozniak, A. S., Bauer, J. E., Sleighter, R. L., Dickhut, R. M., and Hatcher, P. G.: Technical Note: Molecular characterization of aerosol-derived water soluble organic carbon using ultrahigh resolution electrospray ionization Fourier transform ion cyclotron resonance mass spectrometry, Atmos. Chem. Phys., 8, 5099–5111, https://doi.org/10.5194/acp-8-5099-2008, 2008.

Xie, M. J., Mladenov, N., Williams, M. W., Neff, J. C., Wasswa, J., and Hannigan, M. P.: Water soluble organic aerosols in the Colorado Rocky Mountains, USA: composition, sources and optical properties, Sci. Rep.-UK, 6, 39336, https://doi.org/10.1038/srep39339, 2016.

Yee, L. D., Kautzman, K. E., Loza, C. L., Schilling, K. A., Coggon, M. M., Chhabra, P. S., Chan, M. N., Chan, A. W. H., Hersey, S. P., Crounse, J. D., Wennberg, P. O., Flagan, R. C., and Seinfeld, J. H.: Secondary organic aerosol formation from biomass burning intermediates: phenol and methoxyphenols, Atmos. Chem. Phys., 13, 8019–8043, https://doi.org/10.5194/acp-13-8019-2013, 2013.

Yu, L., Smith, J., Laskin, A., Anastasio, C., Laskin, J., and Zhang, Q.: Chemical characterization of SOA formed from aqueous-phase reactions of phenols with the triplet excited state of carbonyl and hydroxyl radical, Atmos. Chem. Phys., 14, 13801–13816, https://doi.org/10.5194/acp-14-13801-2014, 2014.

Zhang, X., Xu, J., Kang, S., Liu, Y., and Zhang, Q.: Chemical characterization of long-range transport biomass burning emissions to the Himalayas: insights from high-resolution aerosol mass spectrometry, Atmos. Chem. Phys., 18, 4617–4638, https://doi.org/10.5194/acp-18-4617-2018, 2018.

Zhao, Y., Hallar, A. G., and Mazzoleni, L. R.: Atmospheric organic matter in clouds: exact masses and molecular formula identification using ultrahigh-resolution FT-ICR mass spectrometry, Atmos. Chem. Phys., 13, 12343–12362, https://doi.org/10.5194/acp-13-12343-2013, 2013.

Zhi, G., Chen, Y., Xue, Z., Meng, F., Cai, J., Sheng, G., and Fu, J.: Comparison of elemental and black carbon measurements during normal and heavy haze periods: implications for research, Environ. Monitor. Assess., 186, 6097–6106, https://doi.org/10.1007/s10661-014-3842-2, 2014.

Zhou, W., Mekic, M., Liu, J., Loisel, G., Jin, B., Vione, D., and Gligorovski, S.: Ionic strength effects on the photochemical degradation of acetosyringone in atmospheric deliquescent aerosol particles, Atmos. Environ., 198, 83–88, 2019.